

# ornl

OAK RIDGE  
NATIONAL  
LABORATORY

MARTIN MARIETTA

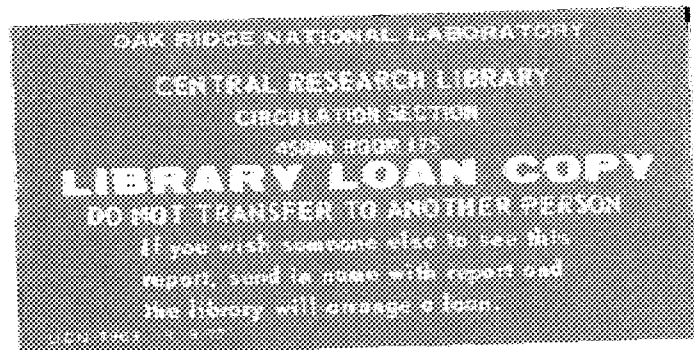
CRNL/TM-11531



3 4456 0314825 2

## A Neutron Spectrometer Based on Optical Detection of $^3\text{He}(n,p)^3\text{H}$ Reactions in a Gas

J. E. Turner  
R. N. Hamm  
T. E. Huston  
H. A. Wright  
W. A. Gibson  
G. S. Hurst



OPERATED BY  
MARTIN MARIETTA ENERGY SYSTEMS, INC.  
FOR THE UNITED STATES  
DEPARTMENT OF ENERGY

This report has been reproduced directly from the best available copy.

Available to DOE and DOE contractors from the Office of Scientific and Technical Information, P.O. Box 62, Oak Ridge, TN 37831; prices available from (615) 576-8401, FTS 626 8401.

Available to the public from the National Technical Information Service, U.S. Department of Commerce, 5285 Port Royal Rd., Springfield, VA 22161.  
NTIS price codes—Printed Copy: A03 Microfiche A01

This report was prepared as an account of work sponsored by an agency of the United States Government. Neither the United States Government nor any agency thereof, nor any of their employees, makes any warranty, express or implied, or assumes any legal liability or responsibility for the accuracy, completeness, or usefulness of any information, apparatus, product, or process disclosed, or represents that its use would not infringe privately owned rights. Reference herein to any specific commercial product, process, or service by trade name, trademark, manufacturer, or otherwise, does not necessarily constitute or imply its endorsement, recommendation, or favoring by the United States Government or any agency thereof. The views and opinions of authors expressed herein do not necessarily state or reflect those of the United States Government or any agency thereof.

CONCEPT FOR  
A NEUTRON SPECTROMETER BASED ON OPTICAL DETECTION  
OF  $^3\text{He}(n,p)^3\text{H}$  REACTIONS IN A GAS

J. E. Turner\*, R. N. Hamm\*, T. E. Huston\*\*, H. A. Wright\*† W. A. Gibson\*,  
and G. S. Hurst\*†

\*Health and Safety Research Division, Oak Ridge National Laboratory, P. O. Box  
2008, Oak Ridge, TN 37830-6123

\*\*Summer participant in Nuclear Energy Research Associates Program sponsored by Oak  
Ridge Associated Universities.

\*Pellissippi International, Inc., 10521 Research Drive, Knoxville, TN 37932

\*†Present address: Consultec Scientific, Inc., Pellissippi Center, Suite 110, 725 Pellissippi  
Parkway, Knoxville, TN 37932-3300

Date Published – June 1990

Prepared for the  
Office of Health and Environmental Research  
Budget Activity No. KP 01 01 00 0

Prepared by the  
OAK RIDGE NATIONAL LABORATORY  
Oak Ridge, Tennessee 37831  
operated by  
MARTIN MARIETTA ENERGY SYSTEMS, INC.  
for the  
U.S. DEPARTMENT OF ENERGY  
under contract DE-AC05-84OR21400





## TABLE OF CONTENTS

Abstract . . . . .	1
1. Introduction . . . . .	2
2. Optical Detector for Charged-Particle Tracks in a Gas . . . . .	2
3. Neutron Spectrometry Based on Observation of ${}^3\text{He}(n,p){}^3\text{H}$ Reactions . . . . .	3
4. Thermal-Neutron Monitoring . . . . .	5
5. Summary . . . . .	6
Appendix . . . . .	6
References . . . . .	14
Figure Captions . . . . .	15
Figures 1 - 11 . . . . .	17
Distribution List . . . . .	28



Concept for a Neutron Spectrometer Based on Optical Detection of  ${}^3\text{He}(n,p){}^3\text{H}$  Reactions in a Gas

J. E. Turner, R. N. Hamm, T. E. Huston, H. A. Wright, W. A. Gibson, and G. S. Hurst

Abstract. The conceptual framework is described for a new type of neutron spectrometer, based on the recently demonstrated principle of optical detection of charged-particle tracks in a gas. Whereas the elastic scattering of a neutron gives rise to the single track of a charged recoil particle, the reaction  ${}^3\text{He}(n,p){}^3\text{H}$  produces an event in which two tracks (those of the proton and triton) diverge from a common vertex at the capture site. The optical detection method, which allows direct visualization of tracks, could be used to distinguish between one- or two-pronged events. The measured total light output from an absorption event would be proportional to  $T_p + T_t$ , the sum of the initial kinetic energies of the proton and triton. Independently of its incident direction, the energy of the absorbed neutron would be given by  $T = T_p + T_t - Q$ , where  $Q = 765$  keV is the energy released by the reaction.

## INTRODUCTION

For the past several years we have been exploring ways to measure the numbers of subexcitation electrons produced along the track of a charged particle in various volume elements that span an ionization chamber. If the charged particle is a recoil nucleus produced by a neutron interaction, then important dosimetric information, such as energy deposited and linear energy transfer (LET) can be inferred from this information<sup>(1,2)</sup>. Hunter has proposed an optical device for making such measurements<sup>(3)</sup>. The principle of operation, which has recently been successfully demonstrated<sup>(4,5)</sup>, is summarized in the next section. In this paper, we show how such a device, incorporating  $^3\text{He}$  in the chamber gas, can be used as a simple, directionally-independent neutron spectrometer.

## OPTICAL DETECTOR FOR CHARGED-PARTICLE TRACKS IN A GAS

A charged particle produces a number of electrons along its path in a gas. These electrons are degraded almost immediately to subexcitation energies, below the threshold for electronic transitions in the gas. In the optical-detection chamber<sup>(3)</sup>, the appearance of a charged particle triggers an externally applied, highly damped RF field ( $\sim 20$  kV and 10 MHz). Before appreciable diffusion occurs, the subexcitation electrons oscillate in response to the field, producing additional local ionizations and excitations of the gas molecules. The net response of the device is the copious emission of photons in all directions from the immediate positions of the individual subexcitation electrons in the particle track. Suitable collection and imaging of the light (e.g., by using two digital vidicon cameras to scan the chamber in perpendicular directions), permits reconstruction of track details for physical analysis.

The detailed design parameters for several gases and chamber components are presented in Ref. (3). We have constructed a preliminary device and demonstrated the

proof of principle by photographing tracks of alpha particles emitted from a radioactive source<sup>(4,5)</sup>. The pictures were made with a chamber containing a mixture of Ar with several percent Xe at a total pressure of 58 kPa (500 torr).

## NEUTRON SPECTROMETRY BASED ON OBSERVATION OF ${}^3\text{He}(n,p){}^3\text{H}$ REACTIONS

The cross sections for neutron interactions with  ${}^3\text{He}$  are shown in Fig. 1. For neutron energies below about 100 keV, the elastic-scattering cross section is smaller than that for the (n,p) reaction. In the MeV range, elastic scattering is more probable. There is, in addition, a small probability (a few percent of the total cross section) that neutron absorption will produce two deuterons, the threshold energy being 4.36 MeV. This reaction will be neglected.

Elastic scattering of a neutron by  ${}^3\text{He}$  in a gas chamber produces a straight-line track of ionizations from the recoil nucleus. In contrast, the (n,p) reaction following neutron absorption produces the two straight tracks of the proton and triton, which emerge from a common vertex at the capture site. Visualization of the tracks in an optical detector exposed to neutrons will enable one to distinguish between the single-pronged elastic-scattering events and the two-pronged absorption events. In the latter case, if the initial kinetic energies of the proton and triton are denoted by  $T_p$  and  $T_t$ , then the energy of the absorbed neutron is given by  $T = T_p + T_t - Q$ , where  $Q = 765$  keV is the energy released by the reaction.

As seen below, with moderate chamber size and gas pressure, most tracks can be contained completely in a gas. The amount of light emitted following an absorption event is then proportional to the number of electrons in the proton and triton tracks<sup>(3)</sup>. Thus the amount of light emitted in a given solid angle is proportional to  $T_p + T_t$ ; its

measurement, therefore, gives the value of  $T$ , the energy of the absorbed neutron. Alternatively, the energies  $T_p$  and  $T_t$  can also be inferred individually from the observed ranges of the particles in the gas in order to obtain  $T$ . (Commonly encountered "wall effects" that occur in conventional proportional counters can be handled in the optical chamber by rejection of events that are seen to involve tracks that intersect a wall.)

As an example, Fig. 2 shows the calculated tracks of the proton and triton following capture of a 500-keV neutron by  $^3\text{He}$  at 29 kPa [250 torr]. (Further study is needed to determine the range of optimum mixtures of He with other gases for the optical chamber. For the present computations we used an available Monte Carlo transport code that we developed earlier<sup>(1)</sup> for particle transport in methane.) In this example, the proton and triton separate in the plane of the figure at an angle  $\alpha = 139^\circ$  with energies  $T_p = 900$  keV and  $T_t = 365$  keV, their sum implying that  $T = T_p + T_t - Q = 900 + 365 - 765 = 500$  keV. The ranges of the proton and triton are, respectively,  $1.7 \times 10^{-3}$  g cm<sup>-2</sup> and  $3.8 \times 10^{-4}$  g cm<sup>-2</sup>, or 7.4 cm and 1.6 cm in the gas at 29 kPa [250 torr]. Such a two-pronged event would be distinguished in the optical chamber from the single-pronged elastic scattering events.

As shown by the kinematic analysis for neutron reactions given in the Appendix, a range of values of the separation angle  $\alpha$  is possible from  $180^\circ$  down to a minimum that depends on the neutron energy  $T$ . As the neutron energy decreases, the minimum value of  $\alpha$  increases, approaching  $180^\circ$ . Thus, with decreasing neutron energy, the vertex becomes generally less and less discernible. In addition, the prongs become generally shorter. Figures 3 and 4 show examples for capture of a 100-keV and a 10-keV neutron at 250 torr. Again, the tracks are in the plane of the figures. In Fig. 4, the vertex is just visible. At the low-energy extreme is capture of a thermal neutron. The proton and triton then come

off "back to back," with the unique energies,  $T_p = 574$  keV and  $T_t = 191$  keV, and  $\alpha = 180^\circ$ . The appearance of the capture event for a thermal neutron is shown in Fig. 5.

These figures illustrate how the appearance of the two-pronged capture event approaches that of a single-prong, as would also result from the elastic scattering of a neutron. For a neutron of energy  $T$ , elastic scattering from  $^3\text{He}$  produces a continuum of recoil energies from zero to  $3T/4$ . Since thermal capture releases 765 keV, all events with light emission below this value are the result of elastic scattering and can be ignored. Moreover, the track of a 765-keV  $^3\text{He}$  recoil nucleus, shown in Fig. 6, is quite different in appearance from Fig. 5, although the same amount of light is emitted. The doubly charged  $^3\text{He}$  nucleus is much more densely ionizing than the singly charged proton and triton.

The tracks in Figs. 2-6 are shown to their best advantage, as it were, in the plane of the figure. Viewed at  $90^\circ$  with respect to this plane, two prongs would appear along the same straight line and could overlap. In order to distinguish clearly between one- and two-pronged cases, each event should be simultaneously observed from at least two mutually perpendicular directions.

#### THERMAL-NEUTRON MONITORING

In some applications, only thermal neutrons are present; and one needs to measure only their fluence or fluence rate. The track produced from capture of a thermal neutron by  $^3\text{He}$  has a unique feature not found in a recoil track produced by elastic scattering. Although the former is also a straight line, it is composed of two segments of different LET that originate from the capture site. This structure can be seen clearly under high resolution, such as that illustrated in Fig. 7, where the pressure is 0.58 kPa [5 torr]. Each dot in the figure represents a subexcitation electron. (In principle, high-resolution digital cameras could also be used with the chamber.) The capture site is near the center of the

figure. The less-dense track of the proton is seen on the right and the more dense track of the triton on the left. For monitoring thermal neutrons with this detector, it is not necessary for the track to be wholly contained in the gas. A straight track with two different LET segments can be differentiated from any elastic recoil track that crosses the chamber.

## SUMMARY

Figures 2-6 indicate that the unique signature of the  ${}^3\text{He}(n,p){}^3\text{H}$  reaction should permit useful measurements of neutron energies over the range from thermal to  $\sim 20$  MeV by optical means. Since the reaction releases 765 keV, a discriminator setting at this level could eliminate a large fraction of the uninteresting elastic-scattering events from analysis. Above that level, the above figures indicate that elastic-scattering events differ markedly in visual appearance from the reactions. The energy resolution would be poorest, of course, for low-energy neutrons. For absorption of a 10-keV neutron, the energy released relative to that for thermal-neutron capture is only  $775/765 = 1.013$ . Above 10 keV, this factor becomes more favorable; the total track length of the proton and triton increases and the two-pronged character of the event becomes more marked (cf. Figs. 3 and 4).

For monitoring slow or thermal neutrons alone, the observation of a track having two distinct LET components, as shown in Fig. 7, should suffice.

## APPENDIX

### Kinematics of ${}^3\text{He}(n,p){}^3\text{H}$ Reaction

Figure 1 gives directly the probabilities for the occurrence of a one- or two-pronged event in  ${}^3\text{He}$  gas exposed to a neutron of given energy  $T$ . In addition, it is of interest to know the probability distributions for proton and triton energies as well as the angles

giving their directions of travel. In this section we give some kinematic details about the reaction under the assumption that the proton and neutron are emitted isotropically in their center-of-mass coordinate system.

Figure 8 represents the conservation of momentum for the reaction as viewed in the laboratory system. The total momentum is that of the neutron before collision,  $(2mT)^{\frac{1}{2}}$ , where  $m$  is the neutron mass. The proton and triton momenta after collision are also shown,  $m_p$  and  $m_t$  being the masses of these particles. The scattering angles of the proton and triton in the lab system are  $\theta$  and  $\phi$ ; the prong angle  $\alpha = \theta + \phi$  as it appears in the lab system is also shown. The conservation of momentum and energy gives the three relations

$$\sqrt{2m_p T_p} \cos \theta + \sqrt{2m_t T_t} \cos \phi = \sqrt{2mT} \quad (1)$$

$$\sqrt{2m_p T_p} \sin \theta = \sqrt{2m_t T_t} \sin \phi \quad (2)$$

$$T_p + T_t = T + Q \quad (3)$$

Quantities in the laboratory and center-of-mass systems are related by means of the velocity-vector diagram shown in Fig. 9. Denoting the neutron and  ${}^3\text{He}$  masses by  $m$  and  $M$  and the neutron velocity by  $v$ , we have for the velocity of the center of mass in the laboratory system

$$v_c = \frac{m v}{m+M} = \frac{\sqrt{2 m T}}{m+M} \quad (4)$$

For given  $T$ , the proton and triton energies  $T_{pc}$  and  $T_{tc}$  in the center-of-mass system are independent of the angles  $\theta_c$  and  $\phi_c$ . This can be seen by writing the conservation equations in the center-of-mass system. From Fig. 9 we see that momentum conservation

requires that

$$\sqrt{2m_p T_{pc}} = \sqrt{2m_t T_{tc}} \quad (5)$$

Energy conservation in the center-of-mass system is expressed by writing

$$T_{nc} + T_{\text{Hec}} = T_{pc} + T_{tc} - Q, \quad (6)$$

where  $T_{nc}$  and  $T_{\text{Hec}}$  are the neutron and  $^3\text{He}$  kinetic energies. Substitution of  $T_{tc}$  from Eq. (6) into Eq. (5) gives

$$T_{pc} = \frac{m_t(T_{nc} + T_{\text{Hec}} + Q)}{m_p + m_t}. \quad (7)$$

In terms of velocities,  $T_{pc} = \frac{1}{2}m_p v_{pc}^2$ ,  $T_{nc} = \frac{1}{2}m(v-v_c)^2$ , and  $T_{\text{Hec}} = \frac{1}{2}Mv_c^2$ . Making these substitutions and solving for  $v_{pc}^2$  gives

$$v_{pc}^2 = \frac{m(v-v_c)^2 + Mv_c^2 + 2Q}{m_p \left[ 1 + \frac{m_p}{m_t} \right]}, \quad (8)$$

showing that the proton energy in the center-of-mass system is the same at all angles and depends only on the neutron energy  $T$ . In terms of this energy,

$$v_{pc}^2 = \frac{2m_t [MT + (m+M)Q]}{m_p(m_p + m_t)(m+M)}. \quad (9)$$

A similar expression holds for  $v_{tc}^2$ , with  $m_p$  and  $m_t$  interchanged.

The relationship between the energies and angles in the two coordinate systems can be found with the help of Fig. 9. For the proton we have

$$v_p \sin \theta = v_{pc} \sin \theta_c \quad (10)$$

and

$$v_p \cos \theta = v_c + v_{pc} \cos \theta_c \quad (11)$$

Taking the ratio of both sides gives

$$\tan \theta = \frac{v_{pc} \sin \theta_c}{v_c + v_{pc} \cos \theta_c} \quad (12)$$

Coupled with Eq. (9), this expression provides a relationship between the proton angle  $\theta$ , the neutron energy  $T$ , and the proton direction  $\theta_c$  in the center of mass system.

Eliminating  $\phi$  and  $T_t$  in Eqs. (1) – (3), one finds that

$$\sqrt{T_p} \cos \theta = \frac{1}{2\sqrt{mm_p T}} [(m_p + m_t) T_p + (m - m_t) T - m_t Q] \quad (13)$$

which relates the proton energy and angle in the lab system for a given neutron energy  $T$ .

Solving Eq. (13), which is quadratic in  $T_p^{1/2}$ , gives

$$\begin{aligned} \sqrt{T_p} = \frac{1}{m_p + m_t} \left\{ (mm_p T)^{1/2} \cos \theta \right. \\ \left. + \left[ mm_p T \cos^2 \theta + (m_p + m_t) \left[ (m_t - m) T + m_t Q \right] \right]^{1/2} \right\} \quad (14) \end{aligned}$$

(Here the positive radical in the quadratic formula has been chosen; setting  $m_p = m_t = m$  and  $Q = 0$  then given the familiar recoil-proton formula,  $T_p = T \cos^2 \theta$ , that characterizes n-p elastic scattering.) Relations analagous to (10) – (14) apply to the triton.

We next consider the probability  $P_p(T_p)dT_p$  that a proton acquires an energy in the range from  $T_p$  to  $T_p + dT_p$ , given the neutron energy  $T$  and assuming that the particles are emitted isotropically in the center-of-mass system. Using this assumption, we may write

$$P_{\theta_c}(\theta_c) d\theta_c = \frac{1}{2} \sin \theta_c d\theta_c = \frac{1}{2} d(\cos \theta_c) \quad . \quad (15)$$

Here  $P_{\theta_c}(\theta_c)$  is the probability density for isotropic emission, which is characterized by a uniform distribution in  $\cos \theta_c$ . For a given value of  $\theta_c$ , one can calculate  $\tan \theta$  from Eqs. (9) and (12), and then obtain  $T_p$  from Eq. (14), thus fixing the scattering event uniquely. For the probability  $P_p(T_p)$ , on the other hand, one has

$$P_p(T_p)dT_p = P_{\theta_c}(\theta_c)d\theta_c = \frac{1}{2} \frac{d(\cos \theta_c)}{dT_p} dT_p \quad . \quad (16)$$

The function  $\cos \theta_c$  can be written out and differentiated explicitly as a function of  $T_p$  after eliminating  $\theta$  from Eqs. (12) and (13). Following this procedure and using the mass values  $m_p = m$  and  $m_t = 3m$  for the reaction, one finds the simple formula

$$P_p(T_p) = \frac{4}{\sqrt{3T(3T+4Q)}} \quad . \quad (17)$$

As with n-p scattering, all possible values of the proton energy are equally probable for a neutron of given energy  $T$ . The kinematic limits on  $T_p$  are given by Eq. (14) with  $\theta = 0^\circ$  (maximum) and  $\theta = 180^\circ$  (minimum):

$$\sqrt{T_{p,\max}} = \frac{\sqrt{T} + \sqrt{9T+12Q}}{4} \quad (18)$$

and

$$\sqrt{T_{p,\min}} = \frac{-\sqrt{T} + \sqrt{9T+12Q}}{4} \quad (19)$$

The function (17) is normalized when integrated between these limits. Similar relations can be found for the triton.

Whereas  $T_p$  can be inferred either from the light output by the proton track or from the range of the proton in the optical chamber, the angle  $\theta$  cannot be measured, since the direction of travel of the neutron is unknown. The angle observed is that between the proton and triton tracks,  $\alpha = \theta + \phi$ . Given  $P_p(T_p)$ , we can obtain the probability distribution in  $\alpha$ ,  $P_\alpha(\alpha)$ , by writing

$$P_\alpha(\alpha)d\alpha = P_p(T_p)dT_p = P_p(T_p) \frac{dT_p}{d\alpha} d\alpha, \quad (20)$$

where it is implied that  $P_p(T_p)$  and  $T_p$  must first be obtained explicitly as functions of  $\alpha$ . Since  $P_p(T_p)$  does not depend on  $\alpha$  [Eq. (17)], we need only to find  $T_p$  as a function of  $\alpha$ . Using Eq. (13) for  $\theta$  and its analogue for  $\phi$  and substituting values for the masses, we have

$$\cos \theta = \frac{4T_p - 2T - 3Q}{\sqrt{2TT_p}} \quad (21)$$

and

$$\cos \phi = \frac{4T_t - Q}{2\sqrt{3TT_t}} \quad (22)$$

These expressions yield

$$\sin \alpha = \sin (\theta + \phi) = \frac{[4TT_p - (2T + 3Q - 4T_p)^2]^{\frac{1}{2}}}{2\sqrt{3T_p(T + Q - T_p)}} \quad (23)$$

This equation, which is quadratic, can be solved for  $T_p$  as a function of  $\sin \alpha$ . After a lengthy calculation of  $dT_p/d\alpha$ , we obtain

$$\begin{aligned} P_\alpha(\alpha) = & \frac{2 \sin \alpha \cos \alpha}{(4 - 3 \sin^2 \alpha) \sqrt{T(9T + 12Q)}} \\ & \times \left\{ \left[ \frac{6}{4 - 3 \sin^2 \alpha} \right] \left[ 5T + 6Q - 3(T + Q) \sin^2 \alpha \right. \right. \\ & \left. \left. \pm \sqrt{3 \cos \alpha \sqrt{3T^2 + 4QT - 3(T + Q)^2 \sin^2 \alpha}} \right] \right. \\ & \left. - 6(T + Q) \pm \frac{\sqrt{3}}{\cos \alpha} \left[ \frac{-6T^2 - 10QT - 3Q^2 + 6(T + Q)^2 \sin^2 \alpha}{\sqrt{3T^2 + 4QT - 3(T + Q)^2 \sin^2 \alpha}} \right] \right\}. \end{aligned} \quad (24)$$

The existence of the two roots for a given neutron energy  $T$  can be understood from Fig. 10. As explained in the caption, even when  $\alpha_1$  and  $\alpha_2$  are the same, the probability for the upper example is not the same as that for the lower. Thus the analytic form for  $P_\alpha(\alpha)$  is different in the two cases. The maximum proton energy  $T_{p,\max}$  occurs when the proton momentum is in forward direction, the same as  $\vec{P}$ . Then  $\alpha = 180^\circ$  ( $\theta = 0^\circ$  and  $\phi = 180^\circ$ ). As  $\theta$  increases, both  $T_p$  and  $\alpha$  decrease, until  $\alpha$  reaches a minimum. Thereafter,  $\alpha$  increases while  $T_p$  continues to decrease until it reaches its minimum value,  $T_{p,\min}$ , when  $\theta = 180^\circ$  and  $\alpha = 180^\circ$ . The proton energy at the minimum prong angle  $\alpha_{\min}$  can be found by differentiating Eq. (23) and solving the equation  $d(\sin \alpha)/dT_p = 0$ . The result is

$$T_{p,\alpha_{\min}} = \frac{(T+Q)(2T+3Q)}{2(T+2Q)} \quad (25)$$

Substitution into Eq. (23) gives for the minimum prong angle for the reaction with a neutron of energy  $T$

$$\sin \alpha_{\min} = \frac{\sqrt{T(3T+4Q)}}{\sqrt{3(T+Q)}} \quad (26)$$

As an example, when  $T = 500$  keV,  $\alpha_{\min} = 157^\circ$  and  $T_{p,\alpha_{\min}} = 662$  keV. We see that, at low neutron energies,  $\sin \alpha_{\min} \gtrsim 0$ ; and so  $\alpha_{\min} \lesssim 180^\circ$ . As the neutron energy increases,  $\alpha_{\min}$  decreases; thus the probability for more evident prong structure increases. For very large  $T$ ,  $\sin \alpha_{\min} \rightarrow 1$ , and so  $\alpha_{\min} \rightarrow 90^\circ$ . The prong angle can never be less than  $90^\circ$ .

The normalized function  $P_\alpha(\alpha)$  is shown by the dashed curve in Fig. 11 for several neutron energies. As explained in the caption, the top solid curve at each energy gives the probability density when the proton is emitted with energy  $T_p < T_{p,\alpha_{\min}}$  and the bottom solid curve gives  $P_\alpha(\alpha)$  when  $T_p > T_{p,\alpha_{\min}}$ . The negative sign in Eq. (24) is used for the former and the positive sign for the latter. The different structure seen in the top solid curve at 10 MeV compared with other energies should be noted. The curve for 50-MeV neutrons (not shown) reveals that, as  $\alpha$  further decreases toward  $\alpha_{\min}$ , the top solid curve goes through a relative maximum at  $\alpha > \alpha_{\min}$  and then increases sharply again when  $\alpha$  approaches  $\alpha_{\min}$ . The curves all diverge when  $\alpha = \alpha_{\min}$ .

## REFERENCES

1. Turner, J. E., Hamm, R. N., Hurst, G. S., Wright, H. A., and Chiles, M. M. *Digital Characterization of Particle Tracks for Microdosimetry*. Radiat. Prot. Dosim. 13 45–48 (1985).
2. Bolch, W. E., Turner, J. E., Hamm, R. N., Wright, H. A., and Hurst, G. S. *A Method of Obtaining Neutron Dose and Dose Equivalent from Digital Measurements and Analysis of Recoil-Particle Tracks*. Health Phys. 53 241–253 (1987).
3. Hunter, S. R. *Evaluation of a Digital Optical Ionizing Radiation Particle Track*. Nucl. Instr. and Meth. A260 469–477 (1987).
4. Turner, J. E., Hunter, S. R., Hamm, R. N., Wright, H. A., Hurst, G. S., and Gibson, W. A. *Digital Characterization of Recoil Charged-Particle Tracks for Neutron Measurements*. Nucl. Instr. and Meth. B40/41 1219–1223 (1989).
5. Turner, J. E., Hunter, S. R., Hamm, R. N., Wright, H. A., Hurst, G. S., and Gibson, W. A. *Development of an Optical Digital Ionization Chamber*. Radiat. Prot. Dosim. 29 9–14 (1989).

## Figure Captions

- Fig. 1. Elastic-scattering and  ${}^3\text{He}(n,p){}^3\text{H}$  reaction cross sections as functions of neutron energy.
- Fig. 2. An example of calculated tracks of the proton and triton for capture of a 500-keV neutron by  ${}^3\text{He}$  in a gas at 29 kPa [250 torr]. The proton and triton tracks are in the plane of the figure, which covers an area 10 cm  $\times$  10 cm. The energies are  $T_p = 900$  keV and  $T_t = 365$  keV, implying that the neutron energy is  $T = 500$  keV. The energy  $T_p + T_t$  can be obtained by measuring the total light output from the chamber in a given direction. Alternatively,  $T_p$  and  $T_t$  can be obtained individually by measuring the proton and triton ranges.
- Fig. 3. Capture of a 100-keV neutron by  ${}^3\text{He}$  at 29 kPa [250 torr]. The calculated tracks are in the plane of the figure.
- Fig. 4. Capture of a 10-keV neutron by  ${}^3\text{He}$  at 29 kPa [250 torr]. The calculated tracks are in the plane of the figure.
- Fig. 5. Thermal-neutron capture by  ${}^3\text{He}$  at 29 kPa [250 torr]. The calculated proton and triton tracks are in the plane of the figure.
- Fig. 6. Calculated track of a 765-keV  ${}^3\text{He}$  recoil nucleus at 29 kPa [250 torr], shown in the plane of the figure.
- Fig. 7. Calculated track from thermal-neutron capture at 0.58 kPa [5 torr], shown in the plane of the figure. The proton (less dense track segment) travels upward toward the right. Each dot represents a subexcitation electron.
- Fig. 8. Conservation of momentum for the reaction  ${}^3\text{He}(n,p){}^3\text{H}$  in the laboratory system.

- Fig. 9. Relationship of the proton and triton velocities  $\vec{v}_p$  and  $\vec{v}_t$  and scattering angles  $\theta$  and  $\phi$  in the laboratory and in the center-of-mass coordinate systems. Here  $\vec{v}_c$  is the velocity of the center of mass in the lab system,  $\vec{v}_{pc}$  and  $\vec{v}_{tc}$  are the velocities of the proton and triton in the center-of-mass system, and  $\theta_c$  and  $\phi_c$  give the directions of the proton and triton in the center-of-mass system.
- Fig. 10. Two ways of conserving momentum for an incident neutron of given momentum  $\vec{P}$ . In the upper example,  $T_p > T_{p,\alpha\min}$ ; in the lower,  $T_p < T_{p,\alpha\min}$ . In either case,  $\vec{P} = \vec{P}_{p1} + \vec{P}_{t1} = \vec{P}_{p2} + \vec{P}_{t2}$ , where  $\vec{P}_{p1}$  and  $\vec{P}_{p2}$  are the proton momenta and  $\vec{P}_{t1}$  and  $\vec{P}_{t2}$  are the triton momenta. When  $\alpha = \alpha_1 = \alpha_2$ , the probability densities for the two examples are different, even though the prong angle is the same.
- Fig. 11. Probability density  $P_\alpha(\alpha)$  as a function of the prong angle  $\alpha$  for neutron energies of 10 MeV, 1 MeV, 100 keV, and 10 keV. The top solid curve for each neutron energy gives  $P_\alpha(\alpha)$  when, as in the lower example in Fig. 10, the proton is emitted with  $T_p < T_{p,\alpha\min}$ . The bottom solid curve gives  $P_\alpha(\alpha)$  when the proton is emitted with  $T_p > T_{p,\alpha\min}$  (upper example in Fig. 10). The sum of the two curves at each neutron energy is the dotted curve, which is normalized to unit area.

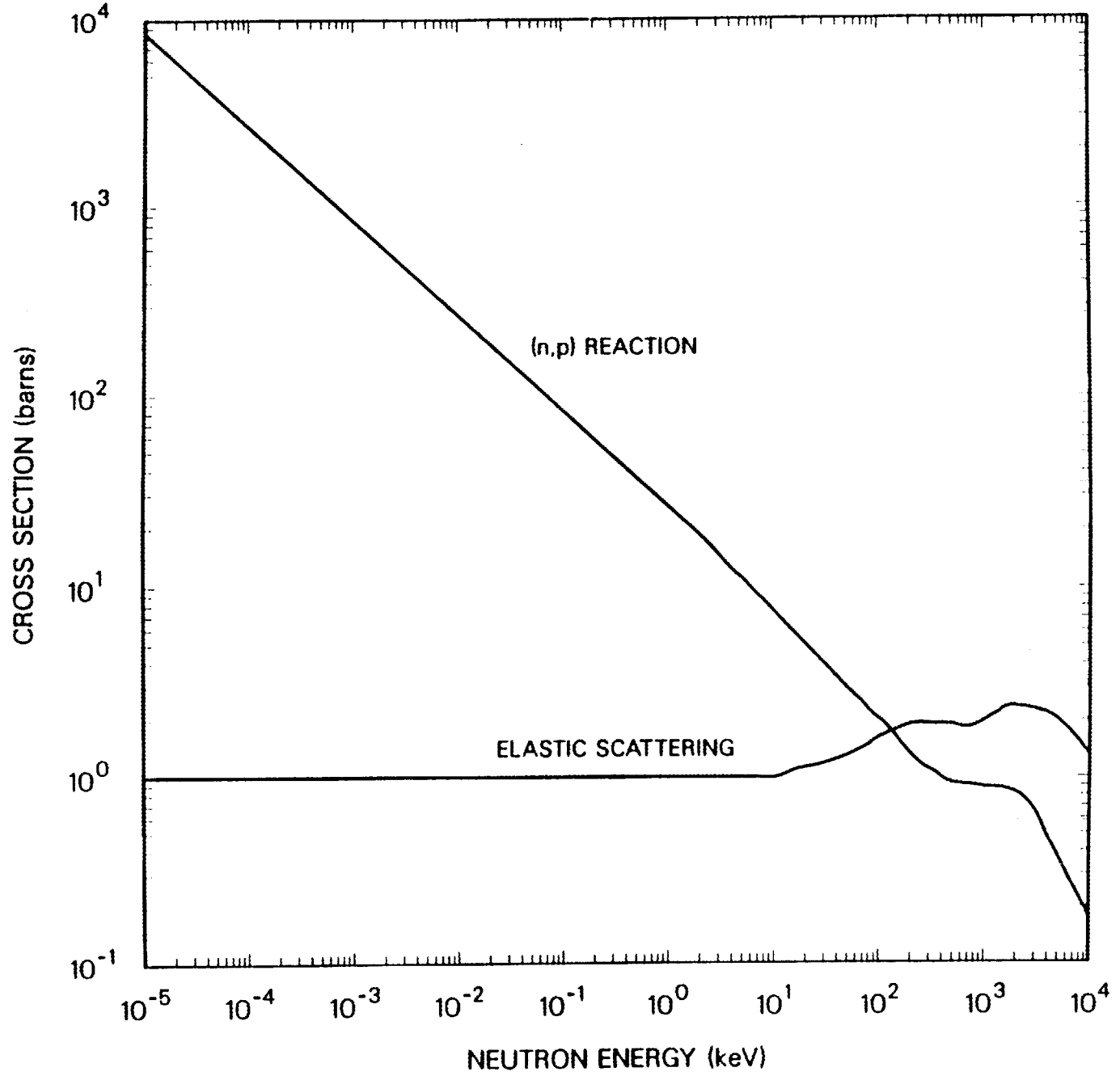


Fig. 1

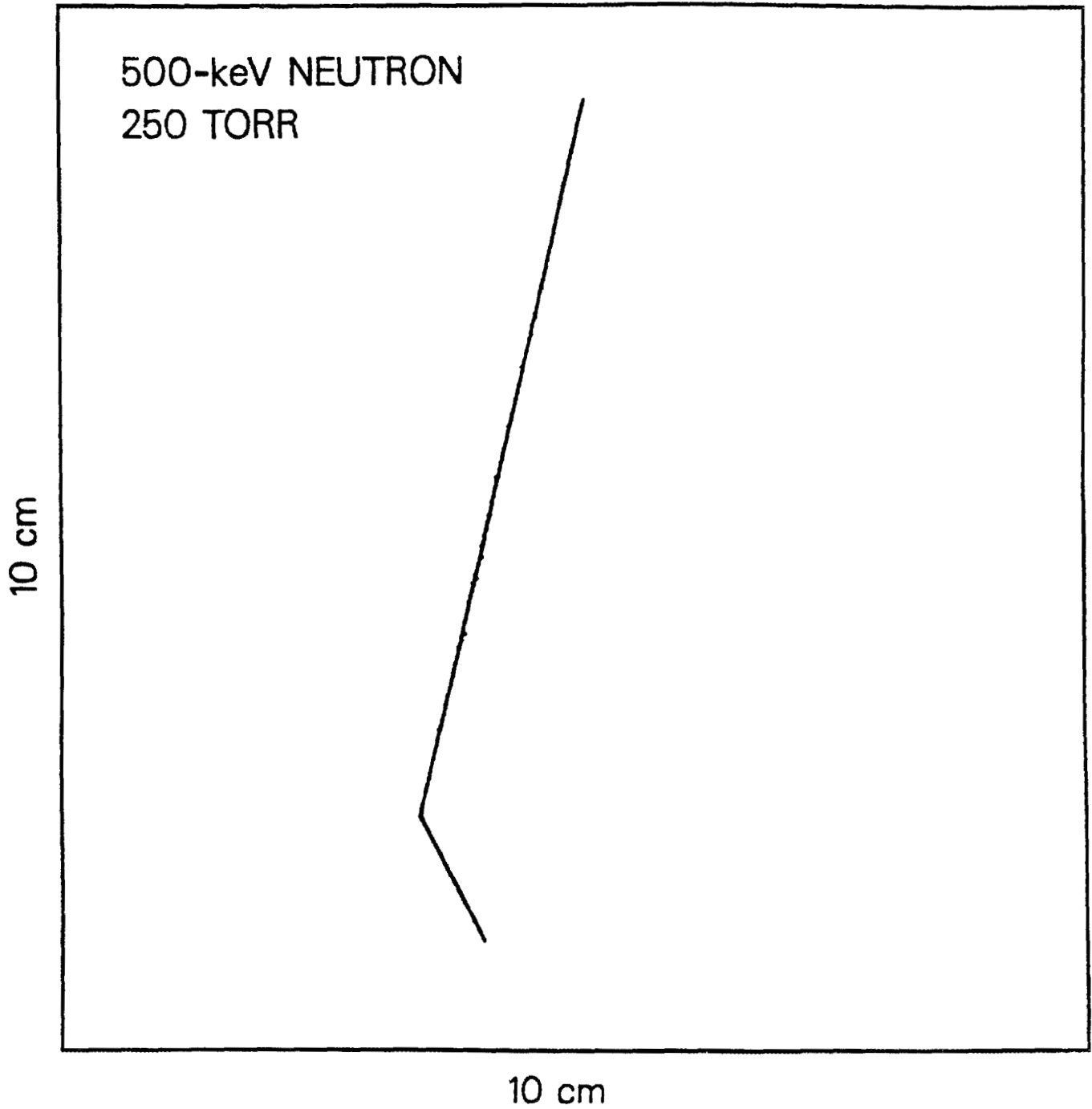


Fig. 2

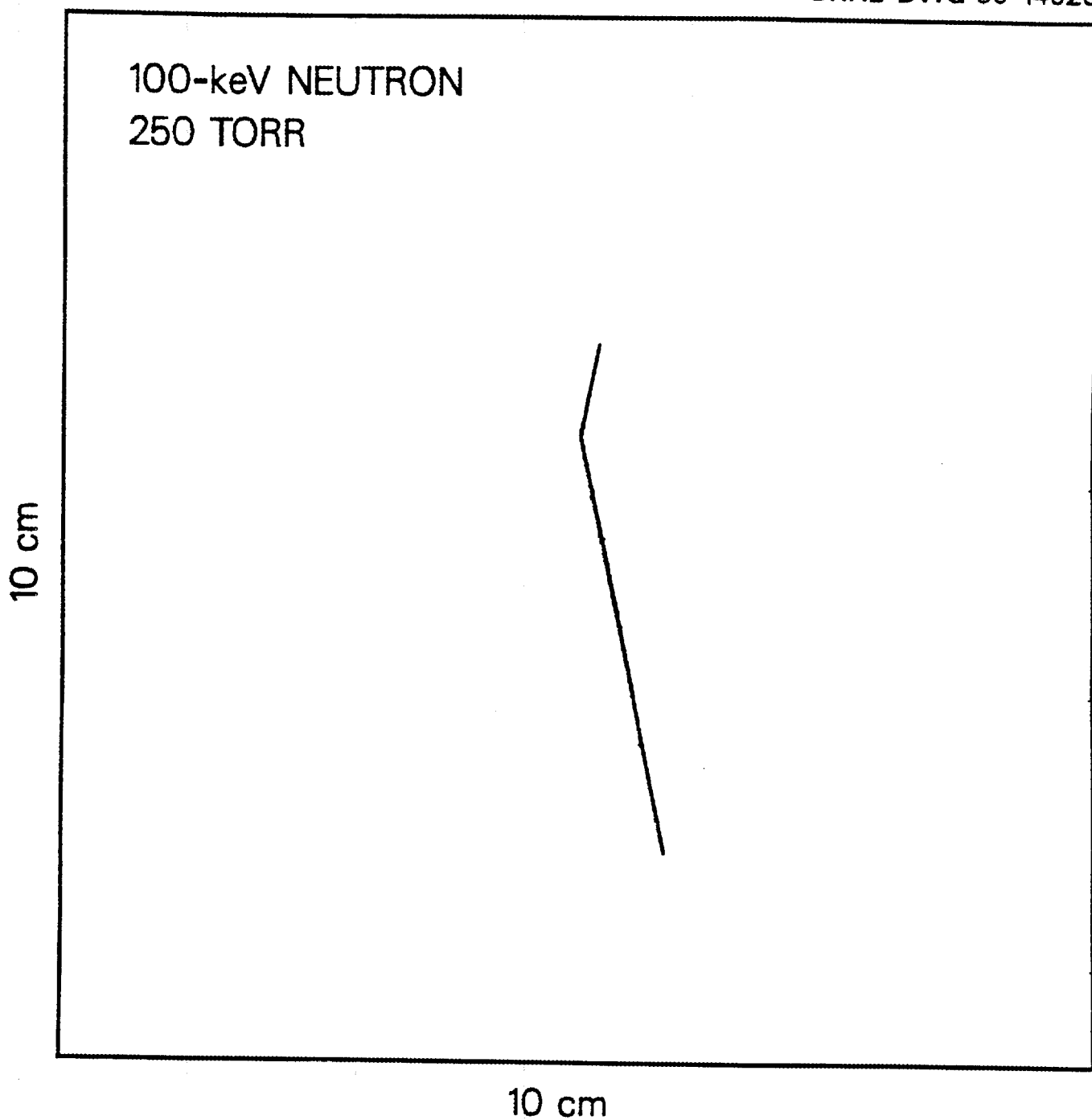


Fig. 3

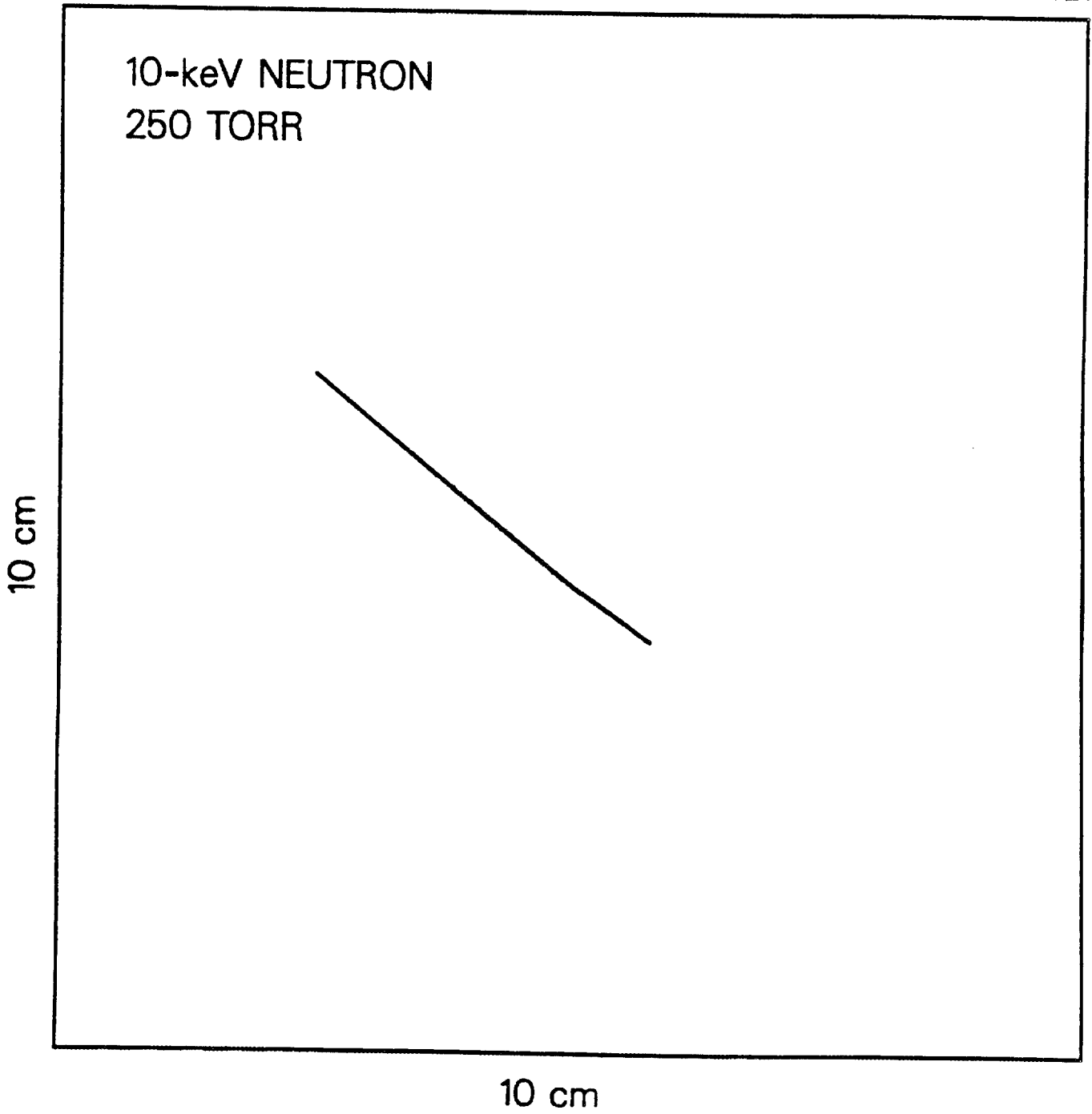


Fig. 4

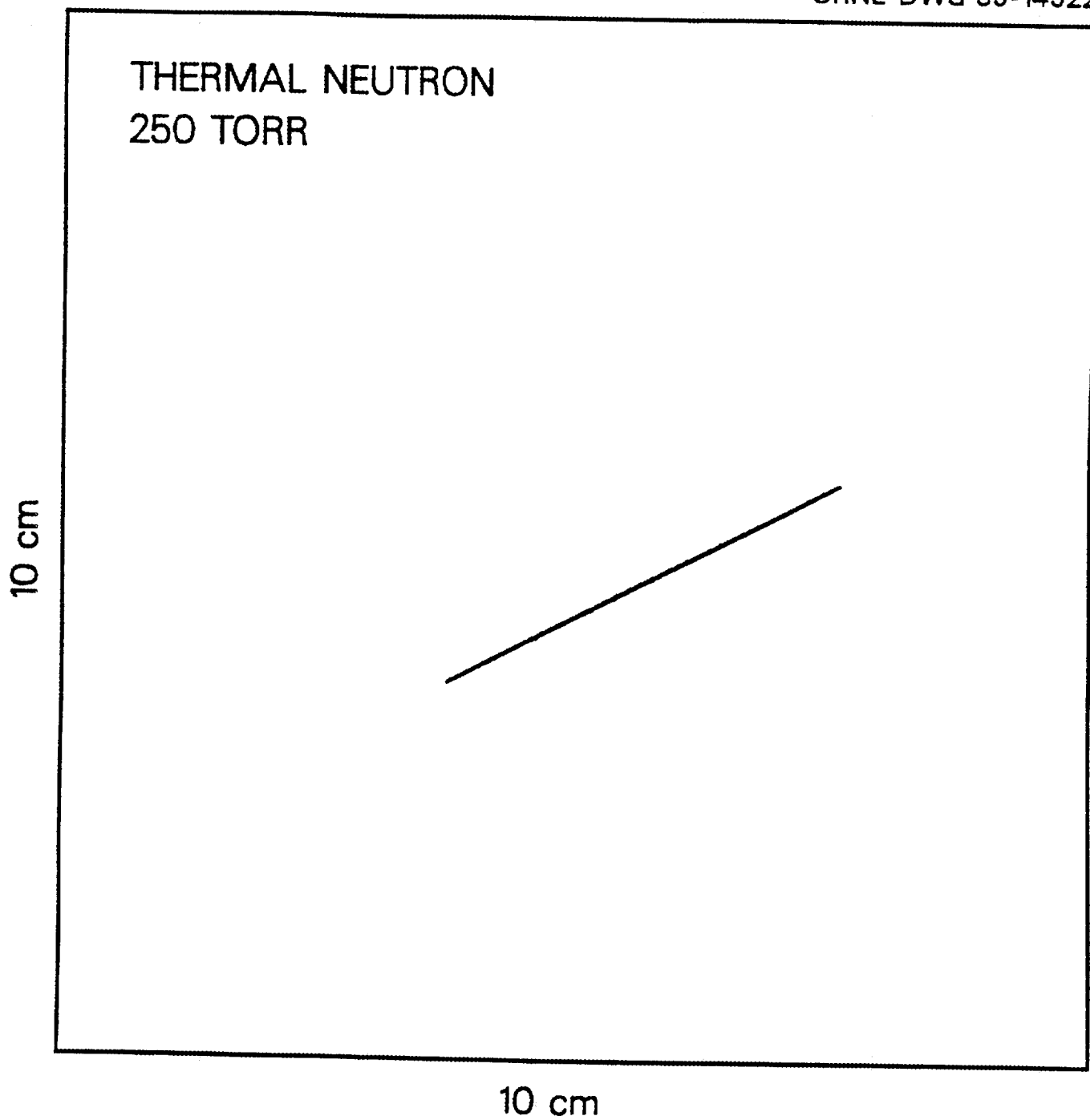


Fig. 5

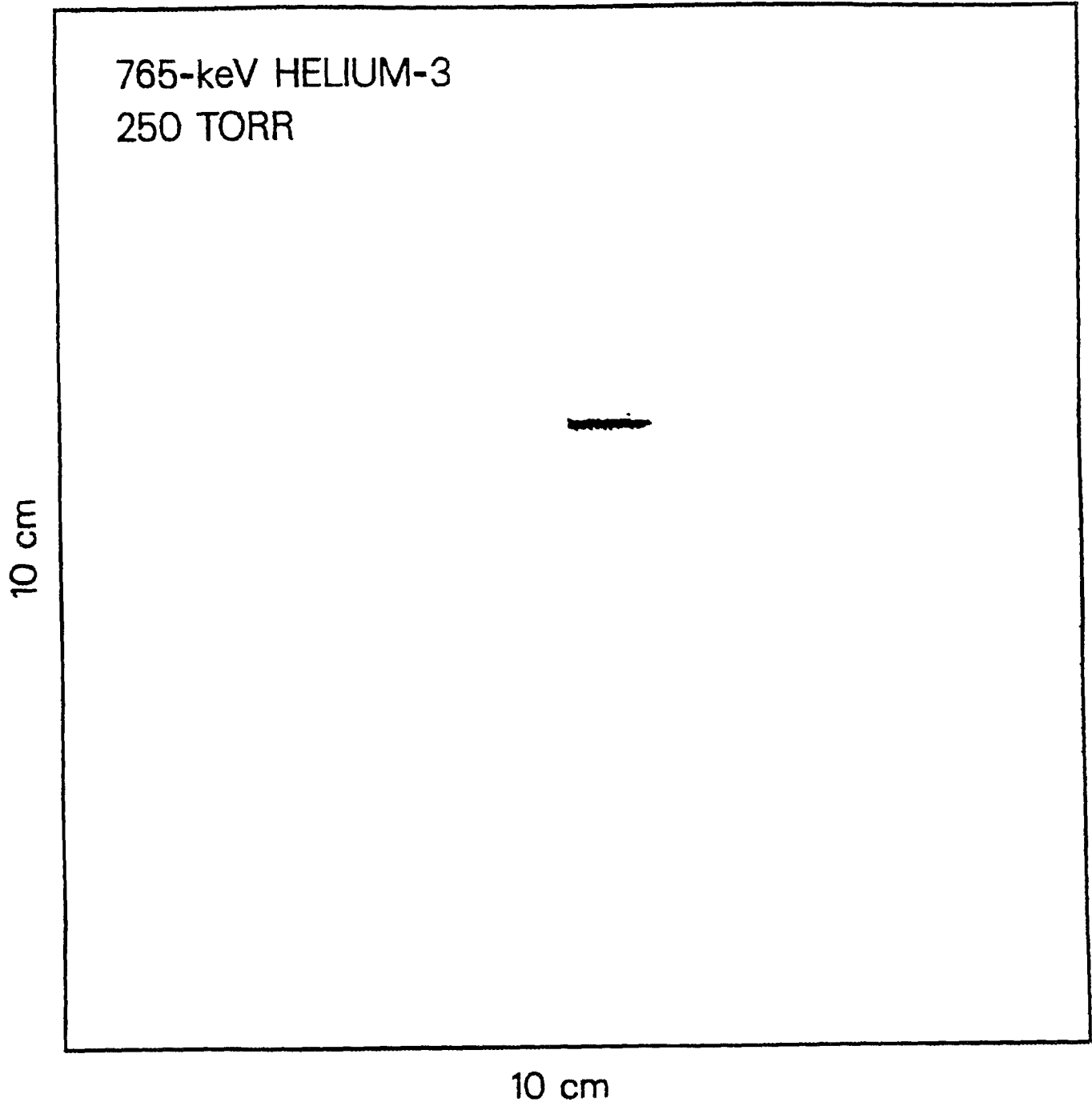


Fig. 6

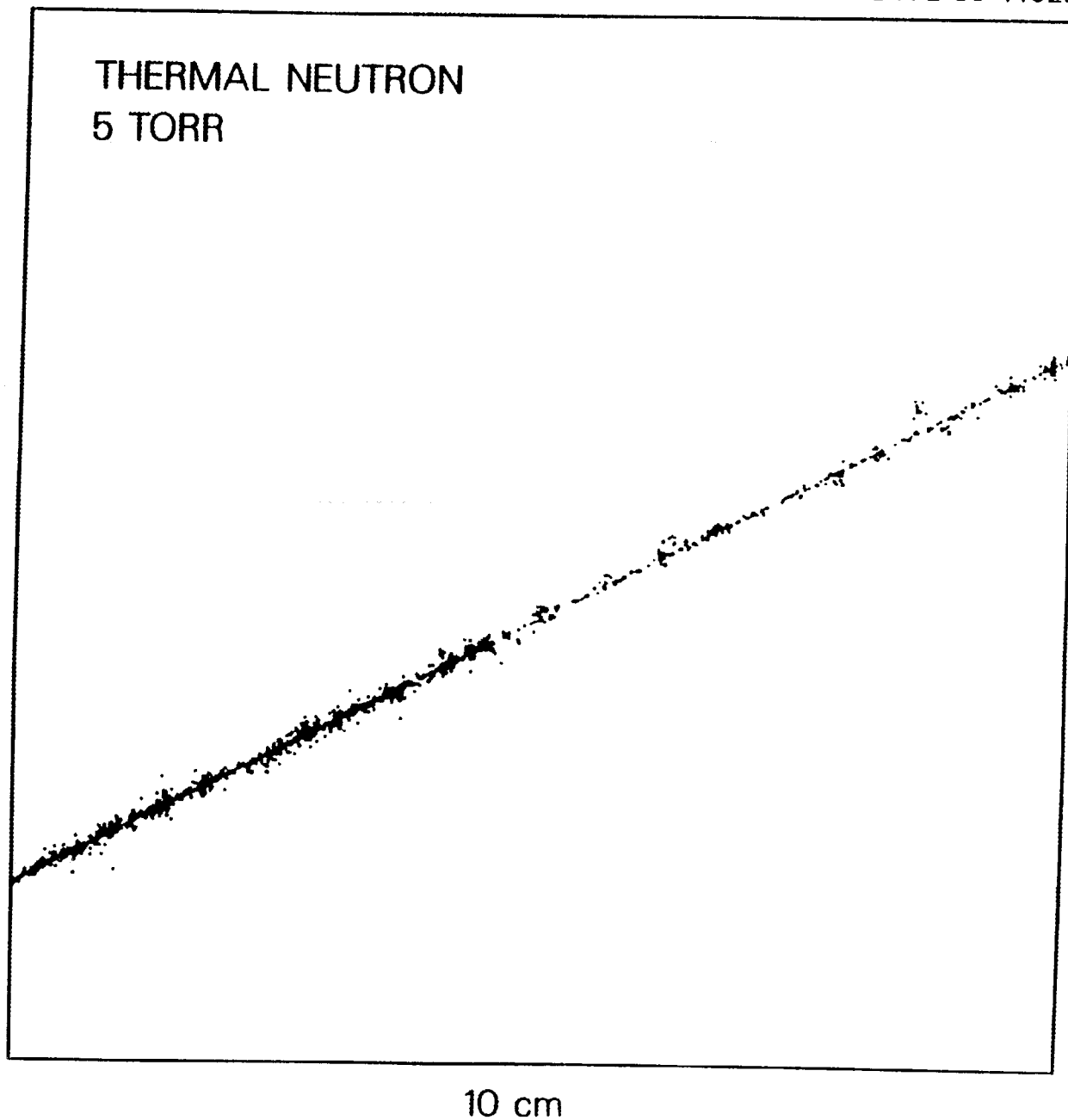


Fig. 7

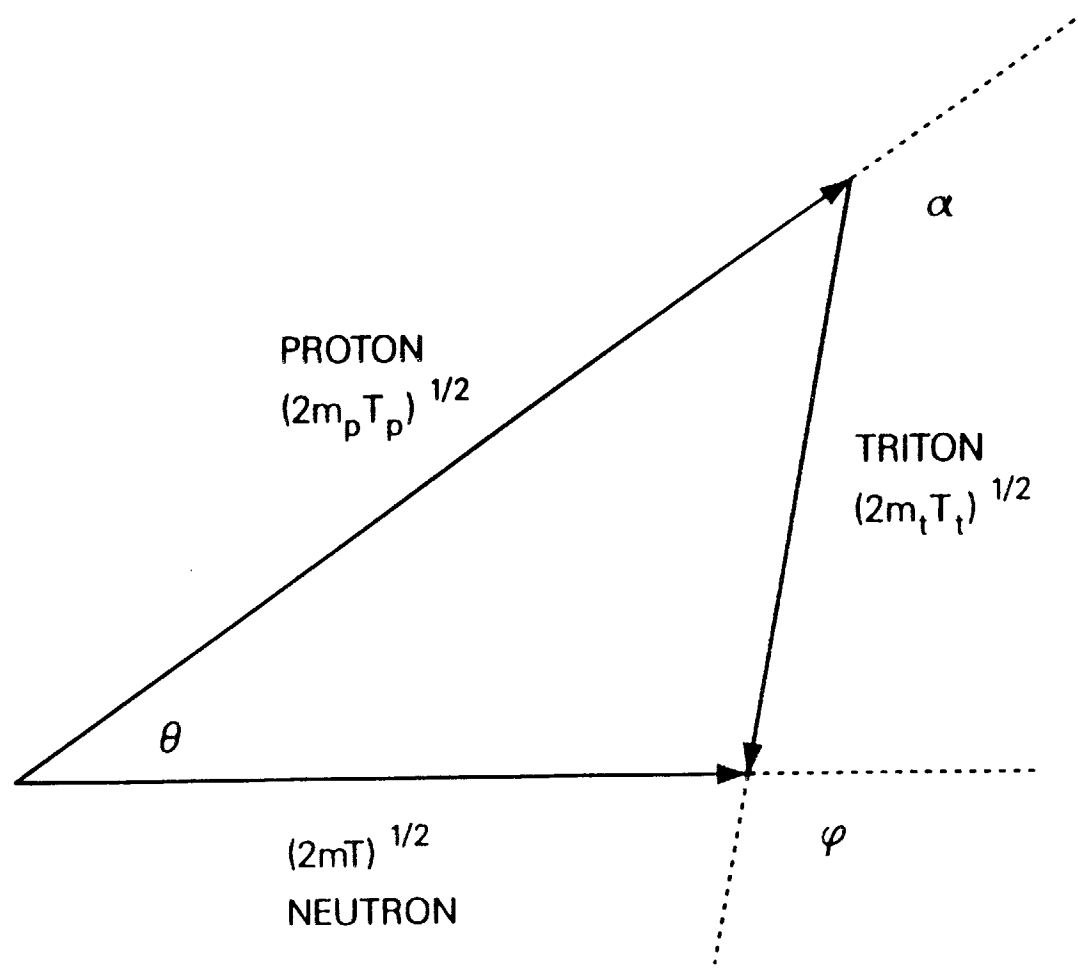


Fig. 8

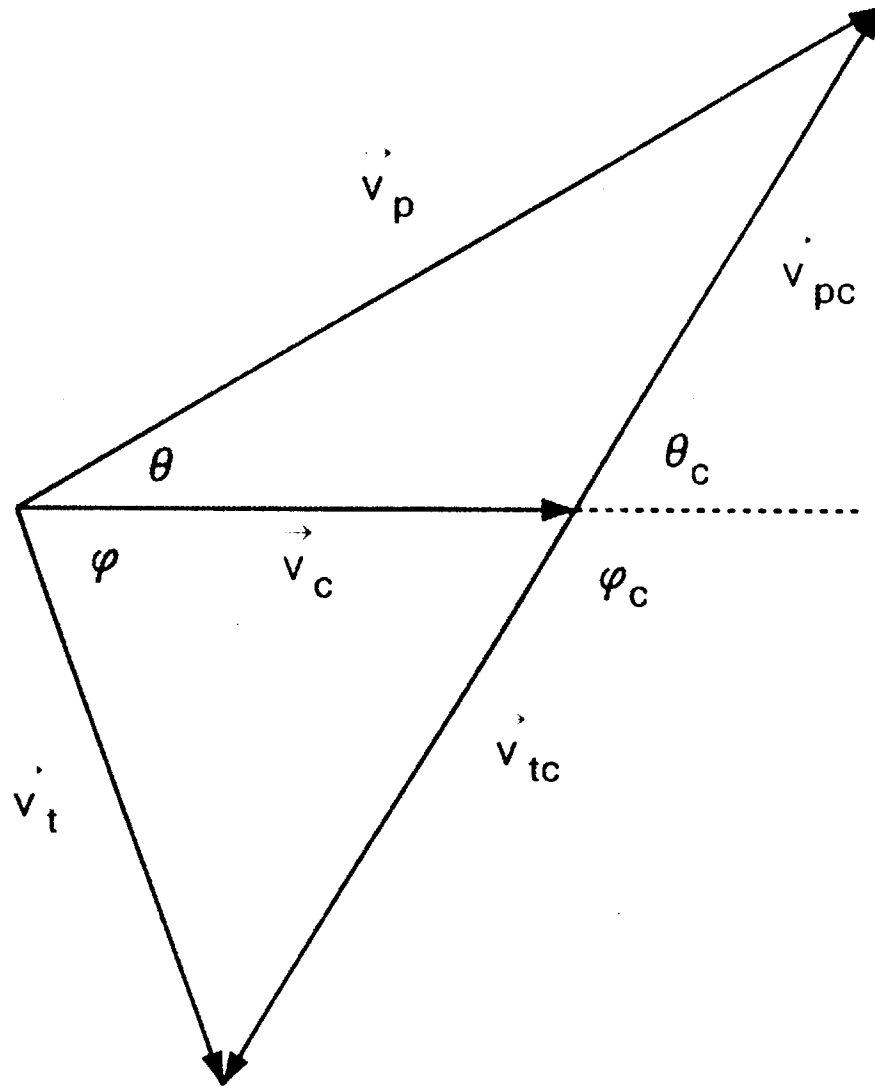


Fig. 9

ORNL-DWG 89-15233

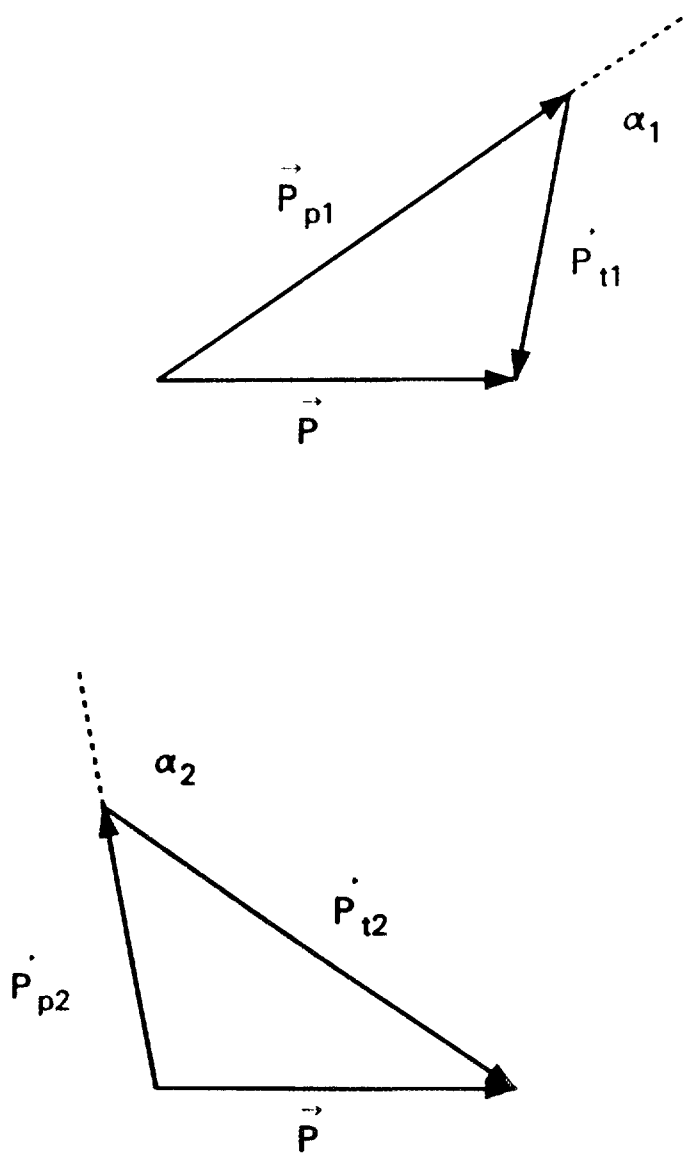


Fig. 10

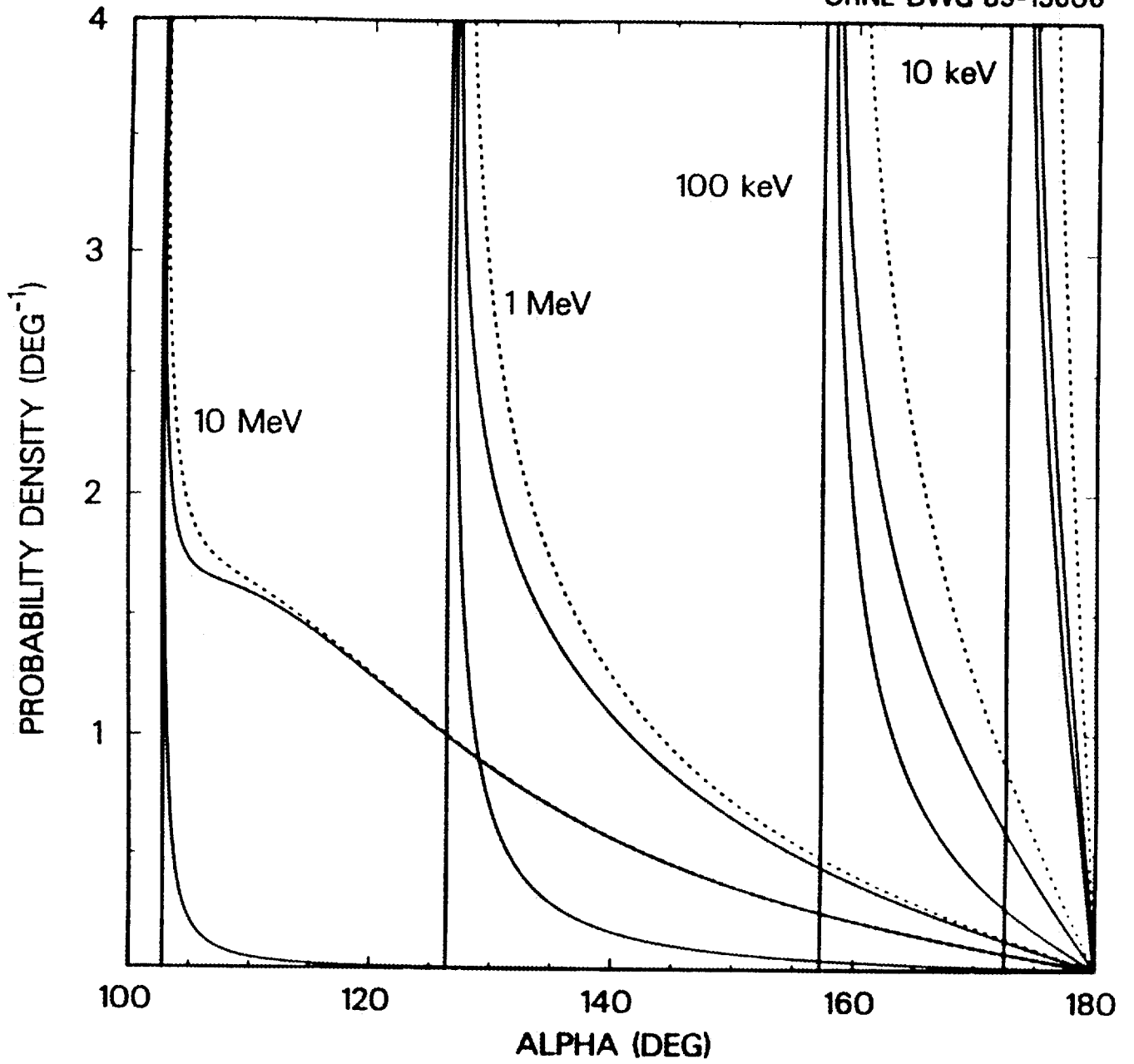


Fig. 11



## INTERNAL DISTRIBUTION

- 1-5. W. A. Gibson
- 6-10. R. N. Hamm
- 11-15. G. S. Hurst
- 16-20. T. E. Huston
- 21-40. J. E. Turner
- 41-45. H. A. Wright
- 46. Central Research Library
- 47. ORNL Y-12 Technical Library
- 48. Document Reference Section
- 49. Laboratory Records
- 50. Laboratory Records-RC
- 51. ORNL Patent Section

## EXTERNAL DISTRIBUTION

- 52. Office of Assistant Manager for Energy Research and Development, Department of Energy, Oak Ridge Operations Office, Oak Ridge, TN 37831
- 53-55. W. E. Bolch, Dept. of Nuclear Engineering, Texas A&M University, College Station, TX 77843-3133
- 56. J. Booz, Institut fuer Medizin, KFA Juelich, Postfach 1913, D-5170, Juelich, Federal Republic of Germany
- 57. R. S. Caswell, National Institute of Standards and Technology, Gaithersburg, MD 20899
- 58. F. Hajnal, U.S. DOE, EML, 376 Hudson Street, New York, NY 10014
- 59. W. M. Lowder, U.S. DOE, EML, 376 Hudson Street, New York, NY 10014
- 60. H. Ing, Chalk River Nuclear Laboratories, Chalk River, Canada
- 61. H. G. Paretzke, GSF, Institute fuer Strahlenschutz, D-8042, Neuherberg, Federal Republic of Germany
- 62. U. Schrewe, Physikalisch-Technische Bundesanstalt, Bundesallee 100, D-3300 Braunschweig, Federal Republic of Germany
- 63. M. Varma, Office of Health and Environmental Research, ER-70, U.S. Department of Energy, Washington, DC 20585
- 64. D. J. Galas, Office of Health and Environmental Research, ER-70, U.S. Department of Energy, Washington, D.C. 20585
- 65-74. Office of Scientific and Technical Information, Oak Ridge, TN 37831